Monthly Notices
of the
ROYAL ASTRONOMICAL SOCIETY

MNRAS **450,** 2500–2505 (2015) doi:10.1093/mnras/stv822

Extracting parameters from colour–magnitude diagrams

C. Bonatto,★ F. Campos, S. O. Kepler and E. Bica

Departamento de Astronomia, Universidade Federal do Rio Grande do Sul, Av. Bento Gonçalves 9500 Porto Alegre 91501-970, RS, Brazil

Accepted 2015 April 10. Received 2015 March 26; in original form 2014 November 19

ABSTRACT

We present a simple approach for obtaining robust values of astrophysical parameters from the observed colour–magnitude diagrams (CMDs) of star clusters. The basic inputs are the Hess diagram built with the photometric measurements of a star cluster and a set of isochrones covering wide ranges of age and metallicity. In short, each isochrone is shifted in apparent distance modulus and colour excess until it crosses over the maximum possible Hess density. Repeating this step for all available isochrones leads to the construction of the solution map, in which the optimum values of age and metallicity – as well as foreground/background reddening and distance from the Sun – can be searched for. Controlled tests with simulated CMDs show that the approach is efficient in recovering the input values. We apply the approach to the open clusters M 67, NGC 6791 and NGC 2635, which are characterized by different ages, metallicities and distances from the Sun.

Key words: Hertzsprung–Russell and colour–magnitude diagrams – open clusters and associations: general.

1 INTRODUCTION

Colour–magnitude diagrams (CMDs) encapsulate important properties of single or composite stellar populations. The most relevant are the age, metallicity, binary fraction and, perhaps, the initial mass function. These are followed by the foreground/background reddening, distance from the Sun, differential reddening (especially for embedded clusters) and even age spread (for young clusters) of the constituent stars. Combined, these parameters contribute – in different degrees – to shaping and defining the CMD morphology of a star cluster. Obviously, the definition of the evolutionary sequences of a single stellar population in a CMD increases with the number of member stars.

A proper or robust determination of astrophysical parameters of star clusters is an important source of constraints for tracing the Galactic structure and understanding its dynamics. Fundamental parameters of young star clusters are important also for studies of dynamical state and cluster dissolution time-scales (e.g. Goodwin 2009; Lamers, Baumgardt & Gieles 2010), *infant mortality*[1] (e.g. Lada & Lada 2003; Goodwin & Bastian 2006), star formation rate in the Galaxy (e.g. Lamers & Gieles 2006; Bonatto & Bica 2011), among others. This kind of analysis started with Trumpler (1930) and continues to date (e.g. Camargo, Bica & Bonatto 2013, and references therein).

In this context, the existence of methods to help in the extraction of parameters from CMDs is fundamental. The simplest approach is to compare a given CMD with those built with stellar populations of previously known parameters. Depending on the quality of the CMD (basically, the definition of the evolutionary sequences), this exercise should yield relative values of the age, distance from the Sun and metallicity. A more quantitative approach is trying to find one isochrone (i.e. a population of stars having the same age and metallicity but different masses) that fits the overall CMD morphology of a star cluster. In principle, this can be – and has been – done *by eye*, but usually restricted to a small number of isochrones. This method is not practical for large sets of isochrones.

However, a deeper interpretation of CMDs in terms of intrinsic cluster properties such as mass, age, metallicity, binary fractions, etc. requires more than estimates or relative quantities. Thus, several approaches have been built for extracting reliable parameters from CMDs of star clusters. For instance, a Bayesian technique to invert CMDs of main-sequence and white dwarf stars has been introduced by von Hippel et al. (2006) and further developed by DeGennaro et al. (2009) and van Dyk et al. (2009). Naylor & Jeffries (2006) apply maximum-likelihood statistics to Hess diagram[2] simulations (including binaries) to derive distances from the Sun and ages. However, they do not consider differential reddening, and their method appears to be more efficient for clusters older than ∼30 Myr. Hillenbrand, Bauermeister & White (2008) model CMDs of star-forming regions and young star clusters by means of varying star formation histories. da Rio, Gouliermis & Gennaro (2010) include differential reddening, age spreads and pre-main-sequence stars to the Naylor

★ E-mail: charles@if.ufrgs.br

[1] Essentially, the early (10−40 Myr) phase in cluster evolution affected by significant disruption processes.

[2] Hess diagrams (Hess 1924) contain the relative density of occurrence of stars in different colour–magnitude cells of the Hertzsprung–Russell diagram.

& Jeffries (2006) method, but have to adopt distance from the Sun and reddening values from previous works. Kerber et al. (2002) use likelihood statistics to identify the synthetic CMD that best reproduces the observed one, with membership probabilities determined from comparison among CMDs extracted from the cluster and a control field. More recently, Bonatto, Lima & Bica (2012) simulated CMDs including cluster (stellar) mass, age, distance modulus (DM), star formation spread, foreground and differential reddening, and binary fraction to reproduce the observed CMDs of young star clusters.

In general, the above approaches are designed to provide a thorough description of the stellar population properties giving rise to an observed CMD. Unfortunately, they usually invoke many free parameters and assumptions; besides, they also tend to overlook some degree of degeneracy associated with, for instance, differential reddening, age spread and binaries. They also do not account for the fact that the low photometric completeness affecting mainly the faint (low-mass) stars – especially at the central region of populous star clusters – may mimic a flat mass function, thus leading to confusion between actual dynamical evolution and completeness effects.

In many – if not most – cases, the interest is just to extract reliable values for the age, metallicity, reddening and distance from the Sun of a star cluster, based only on the observed CMD and a set of isochrones. That is the perspective we will explore in this work.

This paper is organized as follows: in Section 2, we describe the new isochrone fitting approach. In Section 3, we test the parameter recovery efficiency with simulated CMDs. In Section 4, we apply the approach to actual star clusters and discuss the results. Concluding remarks are given in Section 5.

2 FITTING THE HESS DIAGRAM

The first step of the approach consists in building the Hess diagram from the photometric measurements of the observed stars in a given star cluster. As a compromise between resolution and computational time, the Hess diagrams used in this work are built with magnitude and colour cells of dimension $\Delta\,\mathrm{mag} = 0.02$ and $\Delta\,\mathrm{col} = 0.01$, respectively. The smearing effect introduced by photometric uncertainties is explicitly considered in the Hess diagrams. Assuming that uncertainties follow a normal distribution around the mean values, we compute the magnitude and colour fraction (summing for all stars) that occurs in a given cell of the Hess diagram. In practice, this value corresponds to the difference of the error functions computed at the cell borders. Perhaps, this rather continuous nature is the most important advantage of Hess diagrams over the discreteness of CMDs. By definition, the sum of the colour and magnitude density over all Hess cells is the number of input stars.

In short, the present approach consists in finding the isochrone (or range of isochrones) that best maps the high-density ridge occurring along the evolutionary sequences. Quantitatively, this refers to the isochrone that crosses through the largest possible number of high-density cells in the Hess diagram. This measure is quantified by means of the fit index ($f_{\rm ind}$), which contains the total Hess density sum of a given isochrone. Specifically, for an isochrone (characterized by a given age and metallicity) displaced on the Hess diagram by some amount of DM and colour excess (CE), the fit index is quantified as

$$f_{\rm ind} = \sum_{i=1}^{N} H(m_i, c_i), \qquad (1)$$

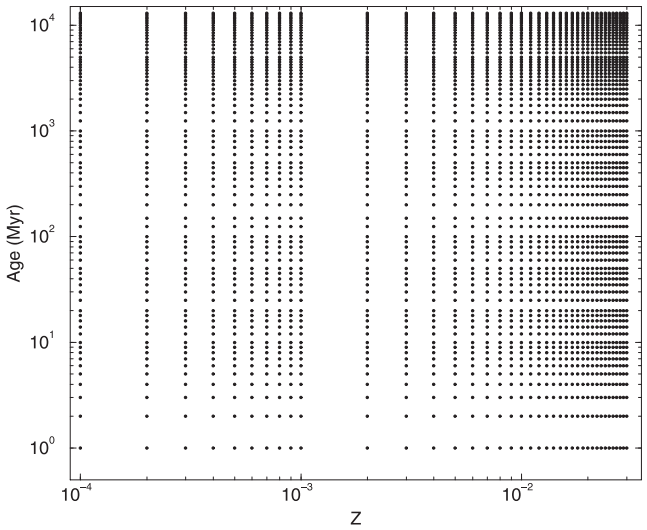

Figure 1. Each point represents an available isochrone built with the corresponding metallicity and age.

where N is the number of magnitude points in the isochrone, m_i and c_i are the magnitude and colour corresponding to the ith isochrone point, and $H(m_i, c_i)$ is the respective Hess density. Additionally, this procedure naturally leads to lower values of $f_{\rm ind}$ for secondary sequences (i.e. lower Hess density) occurring in, e.g. high binary fractions.

Given the wide-range coverage in age, metallicity and mass – and the relative simplicity in obtaining them – we work here with the PARSEC isochrone set (Bressan et al. 2012), version 1.2S.[3] These isochrones are computed for a scaled-solar composition and follow the relation $Y = 0.2485 + 1.78\,Z$. They consider the solar metal content as $Z_{\odot} = 0.0152$. It should be noted that our approach works with any isochrone set, as long as the isochrones cover the ranges of age, metallicity and stellar mass expected to occur in star clusters.

Regarding ages and the total metal content Z, we consider isochrones distributed within $0.0001 \leq Z \leq 0.03$ and ages in the range $1\,\mathrm{Myr} \leq t_{\rm A} \leq 13\,\mathrm{Gyr}$, with higher resolution both for lower metallicity and younger ages. In summary, we work here with a base of 2808 isochrones. For clarity, the distribution of isochrones on the $Z \times$ Age plane is also shown in Fig. 1. Obviously, the approach can be equally used with the full or restricted ranges of metallicity and age.

Once the metallicity and age ranges are selected, each isochrone belonging to those ranges is used to search for the values of apparent DM and CE that produce the best fit to the Hess diagram. In the present context, a fit represents the density sum over all Hess cells crossed by the isochrone (see equation 1). The search ranges for DM and CE must also be given at the start. Thus, our procedure reduces to two the dimensionality of the problem, i.e. finding the best values of DM and CE. This might lead to losing some information on the error propagation in both parameters. However, as discussed in Section 3, the final errors in DM and CE (and the remaining parameters) are computed based on the morphology of the plane $Z \times$ Age as a function of $f_{\rm ind}$. The search for the best values of DM and CE is carried out by the global optimization method known as adaptive simulated annealing (ASA), which is relatively time efficient and

[3] available at *http://stev.oapd.inaf.it/cgi-bin/cmd*.

robust (e.g. Goffe et al. 1994). ASA is able to distinguish and escape from different local maxima in its search for the absolute maximum (e.g. Bonatto et al. 2012).

As a technical caveat, we remark that an isochrone is a discrete set of stellar mass, magnitudes and colour values. But, by construction, the number – and consequently, distribution – of these points is not the same for all isochrones. So, isochrones having a higher number of points would naturally end up being favoured by the present approach. To avoid this, each isochrone is regularized at the start, so that the line connecting two consecutive isochrone points is discretized with the same spacing as that adopted for the Hess cells; additionally, each cell crossed by an isochrone is counted a single time.

The end result of applying the above procedure to all isochrones (belonging to the selected age and metallicity range) is the solution map, which contains the fit index for all values of Z and age. For visualization purposes, this map is first normalized by the $f_{\rm ind}$ corresponding to the best solution. Then, the map resolution is increased by means of a bicubic spline interpolation. The latter step is necessary to find the significant solutions and compute their uncertainties (Section 3). In the context of the present work, a solution would correspond to a region (hotspot) in the map where the highest values of $f_{\rm ind}$ are concentrated. Then, the optimum values of age, metallicity, apparent DM and CE (and, consequently, distance from the Sun) can be derived from the hotspot morphology.

3 TESTING ON SIMULATIONS

In this section, we employ simulated CMDs to investigate the efficiency of our approach in retrieving the input values of relevant astrophysical parameters under very different numbers of stars. The model CMDs correspond to relatively old star clusters with total stellar masses of 250 $M_\odot$(Model#1) and 10 000 $M_\odot$(Model#2), located at 1.1 kpc from the Sun. For the sake of realism, we assume that at this distance, B and V photometry obtained with typical ground-based telescopes would reach apparent magnitudes ∼20 still with relatively small errors.

For consistency with the remainder of this work, photometric errors at given B and V magnitudes are simulated following the average error distribution as a function of magnitude observed for the star clusters M 67, NGC 6791 and NGC 2635 (Section 4). Formally, for stars fainter than $B = 10$ and $V = 10$, the corresponding photometric uncertainties are computed according to $\sigma_B = 0.01 + 1.0 \times 10^{-13} e^{(B/1.1)}$ and $\sigma_V = 0.01 + 1.5 \times 10^{-13} e^{(B/1.2)}$; brighter stars have $\sigma_B = 0.01$ and $\sigma_V = 0.01$. The simulated stellar mass distribution follows a Kroupa (2001) mass function, with each star being attributed B and V magnitude values according to its mass. The mass/light relation was extracted from a specific PARSEC isochrone built according to the Bessell & Brett (Bessell 1990; Bessell & Brett 1998) photometric system.

Except for the total stellar mass, the models are identically built with the isochrone corresponding to 3.5 Gyr of age and total metallicity $Z = 0.012$; additional model parameters are the CE $E(B-V) = 0.21$, and the binary fraction $f_{\rm bin} = 0.3$. At 3.5 Gyr, the corresponding isochrone contains stars in the mass range $0.09 \leq m(M_\odot) \leq 1.4$. For more realism, photometric errors and scatter are also added to the stars. Models#1 and #2 end up having ∼100 and ∼5000 stars brighter than $V = 20$, respectively. The difference in number of stars, as well as the restricted photometric range, is useful for testing the efficiency of the approach under different morphology definition of the evolutionary sequences on the corresponding Hess diagrams.

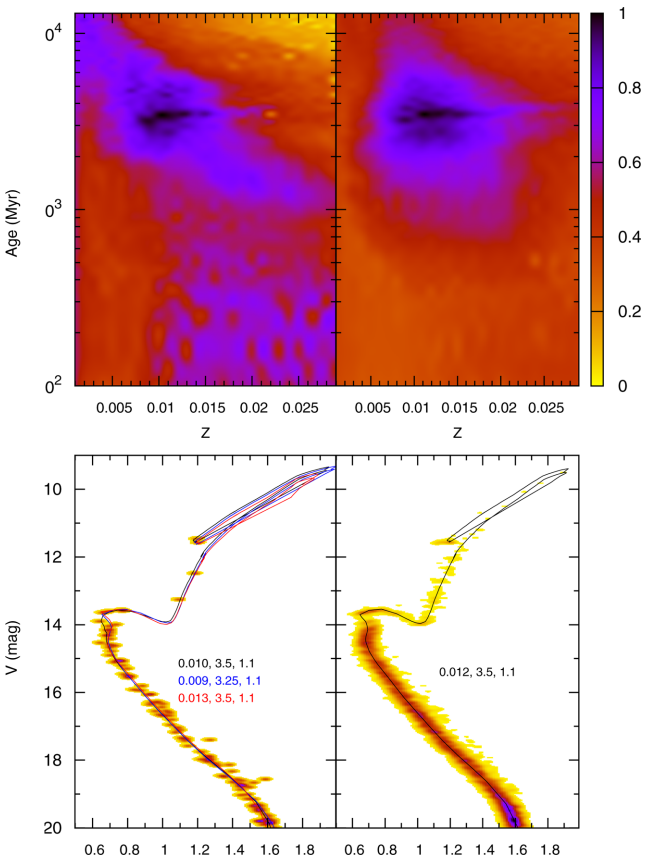

Figure 2. Top: $Z \times$ Age solution maps for Models#1 and #2. The fit index scale is shown by the colour box (top-right). Bottom: $V \times (B-V)$ Hess diagrams together with the best solution isochrones. Isochrone legends show the metallicity (Z), age (Gyr) and distance from the Sun (kpc).

To test the approach, we considered all isochrones having age and metallicity within the ranges 100 Myr-13 Gyr and 0.001–0.030, respectively. Fig. 2 (top panels) shows the normalized, high-resolution solution maps for the three models. Clearly, the convergence pattern on the age × metallicity plane gets tighter as the number of stars (and so, the definition of the evolutionary sequences on the Hess diagram) increases, which should be reflected both on the number of secondary solutions and the scale of the fit parameter uncertainties (see below). As expected, the best solution corresponds to the point with the highest $f_{\rm ind}$ in the map. After locating it, we fit the map with a two-dimensional Gaussian, with axes along the Z and age directions; the values of age and Z at the maximum $f_{\rm ind}$ are kept fixed. The free parameters, the Gaussian amplitude together with Z and age dispersions (σ_Z and $\sigma_{\rm A}$) are searched again with ASA. The best-fitting values of σ_Z and $\sigma_{\rm A}$ are taken as the global uncertainties of Z and age. This Gaussian is subsequently subtracted from the map, and the new (if any) maximum is searched for, thus giving rise to a set of solutions ranked by the respective $f_{\rm ind}$. Each solution corresponds to a single value for DM and CE. Then, considering all solutions occurring within $\pm\sigma_Z$ and $\pm\sigma_{\rm A}$, we compute the weighted (using $f_{\rm ind}$ as weight) average and 1σ dispersion for both DM and CE. As a caveat we remark that, although this approach has the advantage of allowing the detection and characterization of multiple solutions, the $f_{\rm ind}$ morphology around the solutions in Figs 2 and 3 clearly deviate from a simple Gaussianity. The extent to which the deviation affects the parameter uncertainties and alternative approaches for finding errors will be explored in forthcoming work.

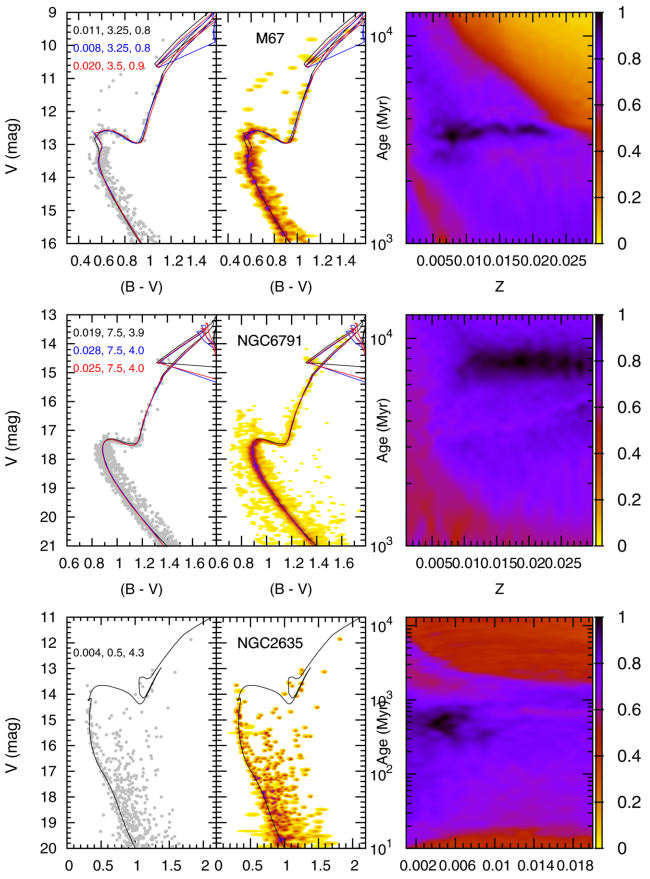

Figure 3. Analysis of M 67 (top panels) and respective model (bottom). Age and metallicity values may differ from those in Table 1 because they correspond to those of the nearest available isochrones. The fit index scale is shown by the colour boxes (right). Isochrone legends show the metallicity (*Z*), age (Gyr) and distance from the Sun (kpc).

The simulated CMDs and respective Hess diagrams are also shown in Fig. 2 (middle and bottom panels), together with the isochrones and parameters corresponding to the best solutions. Since the optimum *Z* and age are searched for on the interpolated, high-resolution map, the numerical values returned do not necessarily coincide with those of the input isochrones.

The best-fitting parameters obtained in the simulations are given in Table 1, where we restrict to solutions having $f_{\rm ind} > 0.7$. Reflecting the low number of stars and, thus, less constrained CMD (and Hess diagram) morphology, Model#1 has three solutions with $f_{\rm ind} > 0.7$. But, they all are consistent with the input values, within the uncertainties.

In summary, tests with simulated CMDs show that our approach is efficient in recovering the input parameters and providing reasonable uncertainties.

4 TESTING ON STAR CLUSTERS

At this point, we test our approach with actual star clusters. For this exercise, we selected the relatively old open clusters M 67 (NGC 2682) and NGC 6791, and the younger NGC 2635. They were selected for having relatively recent and uniform CCD photometry easily accessible through VizieR.[4] In addition, they are characterized by different ages, metallicities, number of stars, distances from the Sun and amount of field-star contamination. Both M 67 and NGC 6791 are older and closer to the Sun and, perhaps, more populous than NGC 2635. One consequence is that both older clusters produce clearly discernible evolutionary sequences in CMDs or Hess diagrams (Fig. 3). NGC 2635, on the other hand, has a more ambiguous (less populated and more contaminated) CMD morphology. Thus, these three clusters provide some variety of conditions for testing our approach.

Table 1. Parameters for models and star clusters. Col. 1: normalized fit index; Col. 2: Age; Col. 3: total metal content; Col. 4: CE; Col. 5: distance from the Sun.

$f_{\rm ind}$	Age (Myr)	Z	$E(B-V)$ (mag)	$d_\odot$ (Kpc)
(1)	(2)	(3)	(4)	(5)
		Model#1 (109 stars)		
1.00	3462 ± 160	0.010 ± 0.001	0.23 ± 0.01	1.07 ± 0.02
0.85	3173 ± 290	0.009 ± 0.001	0.26 ± 0.02	1.07 ± 0.03
0.83	3519 ± 135	0.013 ± 0.001	0.20 ± 0.02	1.11 ± 0.02
		Model#2 (5011 stars)		
1.00	3500 ± 120	0.012 ± 0.001	0.22 ± 0.01	1.08 ± 0.02
		M 67 (446 stars)		
1.00	3292 ± 300	0.008 ± 0.002	0.16 ± 0.03	0.79 ± 0.03
0.82	3542 ± 150	0.019 ± 0.003	0.02 ± 0.02	0.88 ± 0.02
		NGC 6791 (2092 stars)		
1.00	7694 ± 505	0.019 ± 0.001	0.23 ± 0.02	3.87 ± 0.07
0.97	7472 ± 633	0.028 ± 0.002	0.17 ± 0.01	4.03 ± 0.06
0.85	7556 ± 250	0.025 ± 0.001	0.18 ± 0.02	4.02 ± 0.06
0.78	8000 ± 440	0.012 ± 0.001	0.29 ± 0.02	3.67 ± 0.07
		NGC 2635 (481 stars)		
1.00	500 ± 100	0.004 ± 0.001	0.39 ± 0.02	4.28 ± 0.15

4.1 M 67

The high Galactic latitude of M 67 ($b = +31.9^\circ$) is an advantage for minimizing field-star contamination, which makes it a convenient cluster for this analysis. Several works have come up with a nearly solar metallicity for M 67 (e.g. Sarajedini, Dotter & Kirkpatrick 2009). The WEBDA[5] data base provides $d_\odot = 0.91$ kpc, $E(B-V) = 0.06$, and the 2.6 Gyr of age. More recently, the study of Chen et al. (2014) assumed $Z = 0.02$, $(m - M)_o = 9.75$, and $E(B-V) = 0.03$, with which they derived the significantly older value of 3.5 Gyr as the most probable age of M 67.

Our CMD of M 67 consists of *B* and *V* photometry taken from the ground-based CCD astrometry catalogue of Yadav et al. (2008). We selected stars lying closer than 20 arcmin from the cluster centre, thus resulting in 446 stars brighter than $V = 16$. As expected, the evolutionary sequence of a relatively old open cluster stands out clearly in the CMD and Hess diagram, with a minimum field contamination (Fig. 3).

Solutions have been searched for isochrones having age within 1−13 Gyr and metallicity within 0.001–0.03. Our approach finds two solutions having $f_{\rm ind} > 0.7$ for M 67. The results are given in Table 1, and the corresponding solution maps, Hess diagrams and CMDs are shown in Fig. 3. The solution map pattern shows a rather tight distribution of ages around ∼3.5 Gyr, but the metallicity distributes over the relatively wide range $0.06 \lesssim Z \lesssim 0.22$. Within the

[4] http://vizier.u-strasbg.fr/viz-bin/VizieR

[5] http://www.univie.ac.at/webda/

uncertainty, the age we find for M 67 – corresponding to the best fit – is nearly the same as that found by Chen et al. (2014), but our metallicity is about half theirs. The second-ranked solution is rather consistent in age, but presents an increase in metallicity. Interestingly, the isochrone fit adopted by Chen et al. (2014) is recovered by our approach as the second-ranked solution, with $f_{\rm ind} = 0.82$. For comparison purposes, Fig. 3 shows the two solutions superimposed to the CMD and Hess diagram of M 67.

4.2 NGC 6791

NGC 6791 is closer to the Galactic plane ($b = +10.^{\circ}9$) and somewhat older and metal richer than M 67. For instance, WEBDA gives $d_{\odot} = 4.1$ kpc, $E(B-V) = 0.12$, 4.4 Gyrand $Z = 0.21$ for NGC 6791. More recently, van den Berg et al. (2014, and references therein) use [Fe/H] ~ 0.3 (thus implying $Z \sim 2Z_{\odot}$) and derive an age of $\sim$8 Gyr for NGC 6791.

The B and V photometry for NGC 6791 was taken from the CCD catalogue of Stetson, Brunt & Grundahl (2003). To minimize field-star contamination, we only considered stars closer than 3 arcmin from the centre and brighter than $V = 21$, resulting in $\sim$2100 stars. Even so, the CMD and Hess diagram of NGC 6791 clearly contain some degree of field contamination (Fig. 3).

Solutions were searched within the same age and metallicity ranges as for M 67. We find four solutions having $f_{\rm ind} > 0.7$ for NGC 6791, and they all consistently confirm its older age with respect to M 67, probably reaching 8 Gyr. Regarding the metallicity, the highest ranked solutions indicate $0.019 < Z < 0.028$, but with a value as low as $Z = 0.012$ with a low probability. Thus, the metallicity appears to be higher than solar, probably reaching nearly twice the solar value (Table 1). These features (i.e. the relatively narrow age range associated with some dispersion in metallicity) are present in the solution map.

The three best-fitting PARSEC isochrones produce an excellent description of the entire evolutionary sequence of NGC 6791. However, the difference in $f_{\rm ind}$ among the first three solutions is rather small, which means that they are statistically significant as well. The weighted average of the four solutions (using the respective $f_{\rm ind}$ as weight) yields the age 7668 ± 193 Myr, $Z = 0.021 \pm 0.006$, $E(B-V) = 0.21 \pm 0.05$ and $d_{\odot} = 3.90 \pm 0.14$ kpc. An age between 7.5 and 8 Gyr (in our case derived for most of the main sequence and RGB+AGB stars) is consistent with the value obtained by García-Berro et al. (2010) based on properties of the white dwarf cooling sequence of NGC 6791.

4.3 NGC 2635

Located in the third Galactic quadrant and at $b = +3.^{\circ}96$, the field of NGC 2635 is naturally more contaminated than both of M 67 and NGC 6791. Combined with a large distance from the Sun and a small population, the available CMDs of NGC 2635 lead to somewhat discrepant values of its fundamental parameters. For instance, WEBDA provides $\sim$300 Myr of age, $d_{\odot} = 5.7$ kpc, and $E(B-V) = 0.35$. Moitinho et al. (2006) employ CCD broad-band photometry and CMDs to find $\sim$600 Myr of age $d_{\odot} \sim 4$ kpc, $E(B-V) = 0.35$ and the very low metallicity $Z = 0.004$ for NGC 2635.

Photometry for NGC 2635 was taken from the CCD broad-band UBV catalogue of Moitinho et al. (2006), via VizieR. Because of the previous evidence of a younger age and lower metallicity (with respect to M 67 and NGC 6791), solutions have been searched for isochrones with age within 10 Myr−13 Gyr and metallicity within 0.001–0.02.

The CMD and Hess diagram of NGC 2635 clearly reflect its small stellar content (e.g. the rather discrete distribution of stars along the main sequence) and unaccounted for field-star contamination. Nevertheless, our approach indicates $\sim$500 Myr as the most probable age for NGC 2635, together with the low metallicity of $Z = 0.004$. Interestingly, this age corresponds to the average between those of WEBDA and Moitinho et al. 2006). Metallicity, reddening and distance from the Sun agree with those of Moitinho et al. (2006). The best-fitting isochrone passes through the main sequence and a group of relatively red and bright stars that – in this case – would correspond to giants (Fig. 3). It is obvious that, if some field-star contamination is present among the giants, the end result of the age may change, but still probably within the 100 Myr uncertainty derived by our approach. Nevertheless, the $f_{\rm ind}$ map shows that age and metallicity are quite concentrated around $\sim$500 Myr and $Z = 0.004$.

Finally, we note that the fit index patterns in the solution maps of M 67 and NGC 6791 present a high degree of similarity. Basically, they are relatively constrained in age but somewhat wide in metallicity, which explains the Z-distribution among the solutions for M 67 and NGC 6791 (Table 1). The apparent degeneracy in metallicity associated with isochrones – especially the old ones – is a clear example of the difficulties related to deriving precise values of Z from photometry. Ideally, isochrones covering a wider range of wavelengths – especially towards the blue/violet – should mitigate this degeneracy and, as discussed in previous sections, our approach is designed to work with any isochrone set. However, isochrones built with blue filters usually do not yet have the same accuracy as those in B and V in describing observed evolutionary sequences in CMDs. This occurs especially because of the lack of a robust determination of molecular opacities, incorrect bolometric corrections and colour–$T_{\rm eff}$ relations, and incomplete convection description, mostly related to low $T_{\rm eff}$. This issue is explored and highlighted, for instance, in Campos et al. (2013), and references therein.

5 SUMMARY AND CONCLUSIONS

In this paper, we describe a relatively simple and direct approach designed to extract astrophysical parameters (specifically the age, metallicity, foreground reddening and distance from the Sun) from CMDs of star clusters. Central to the approach is the availability of isochrone data bases covering wide ranges – and with a high resolution – in age and metallicity. For this reason, we work here with the PARSEC (Bressan et al. 2012) isochrone data base, but any comprehensive (in terms of age and metallicity) isochrone set should work as well.

The basic idea is to search for the isochrone that best maps the high-density regions of the Hess diagram corresponding to the input CMD. This is accomplished by varying the apparent DM and reddening for each isochrone. At each step, the fit index ($f_{\rm ind}$) corresponding to the sum of the Hess density spanned by the isochrone is computed. The best values of DM and reddening are those that lead to the highest possible $f_{\rm ind}$ for each isochrone. Finally, a map of $f_{\rm ind}$ is produced on the age × metallicity plane, in which the solutions and uncertainties are searched for.

Tests with simulated CMDs show that the approach is efficient in recovering the input values. Obviously, convergence (and uncertainties) depends somewhat on the Hess diagram morphology. Star cluster CMDs containing large number of member stars tend to produce well-defined evolutionary sequences in Hess diagrams. This, in turn, increases convergence of the approach and decreases the uncertainties in the retrieved parameters.

From a theoretical perspective, it is clear that our approach depends critically on the accuracy of the isochrones in describing the stellar evolutionary sequences at a given age and metallicity. Right now this is a minor issue, because several groups are actively working on the development of isochrones based on state-of-the-art stellar physics.

ACKNOWLEDGEMENTS

We thank an anonymous referee for important comments and suggestions. Partial financial support for this research comes from CNPq (Brazil). This research has made use of the VizieR catalogue access tool, CDS, Strasbourg, France. This research has made use of the WEBDA data base, operated at the Department of Theoretical Physics and Astrophysics of the Masaryk University.

REFERENCES

Bessell M. S., 1990, PASP, 102, 1181
Bessell M. S., Brett J. M., 1988, PASP, 100, 1134
Bonatto C., Bica E., 2011, MNRAS, 415, 2827
Bonatto C., Lima E. F., Bica E., 2012, A&A, 540, A137
Bressan A., Marigo P., Girardi L., Salasnich B., Dal Cero C., Rubele S., Nanni A., 2012, MNRAS, 427, 127
Camargo D., Bica E., Bonatto C., 2013, MNRAS, 432, 3349
Campos F., Kepler S. O., Bonatto C., Ducati J. R., 2013, MNRAS, 433, 243
Chen Y., Girardi L., Bressan A., marigo P., Barbieri M., Kong X., 2014, MNRAS, 444, 2525
Da Rio N., Gouliermis D. A., Gennaro M., 2010, ApJ, 723, 166
DeGennaro S., von Hippel T., Jeffreys W. H., Stein N., van Dyk D., Jeffrey E., 2009, ApJ, 696, 12
García-Berro E. et al., 2010, Nature, 465, 194
Goffe W. L., Ferrier G. D., Rogers J., 1994, J. Econometrics, 60, 65
Goodwin S. P., 2009, Ap&SS, 324, 259
Goodwin S. P., Bastian N., 2006, MNRAS, 373, 752
Hess R., 1924, Die Verteilungsfunktion der absol. Helligkeiten etc. Probleme der Astronomie. Festschrift fur Hugo v. Seeliger. Springer, Berlin, p. 265
Hillenbrand L. A., Bauermeister A., White RJ., 2008, in van Belle G., ed., ASP Conf. Ser. Vol. 384, 14th Cambridge Workshop on Cool Stars, Stellar Systems, and the Sun. Astron. Soc. Pac., San Francisco, p. 200
Kerber L. O., Santiago B. X., Castro R., Valls-Gabaud D., 2002, A&A, 390, 121
Kroupa P., 2001, MNRAS, 322, 231
Lada C. J., Lada E. A., 2003, ARA&A, 41, 57
Lamers H. J. G. L. M., Gieles M., 2006, A&A, 455, L17
Lamers H. J. G. L. M., Baumgardt H., Gieles M., 2010, MNRAS, 409, 305
Moitinho A., Carraro G., Baume G., Vázquez R. A., 2006, MNRAS, 367, 1441
Naylor T., Jeffries R. D., 2006, MNRAS, 373, 1251
Sarajedini A., Dotter A., Kirkpatrick A., 2009, ApJ, 698, 1872
Stetson P. B., Brunt H., Grundahl F., 2003, PASP, 115, 413
Trumpler R. J., 1930, Lick Obs. Bull., 14, 154
van den Berg D. A., Bergbusch P. A., Ferguson J. W., Edvardsson B., 2014, ApJ, 794, 72
van Dyk D., DeGennaro S., Stein N., Jeffreys W. H., von Hippel T., 2009, Ann. Appl. Stat., 3, 117
von Hippel T., Jeffreys W. H., Scott J., Stein N., Winget D. E., DeGennaro S., Dam A., Jeffrey E., 2006, ApJ, 645, 1436
Yadav R. K. S. et al., 2008, A&A, 484, 609

This paper has been typeset from a TEX/LATEX file prepared by the author.